https://doi.org/10.5194/amt-2022-157
Preprint. Discussion started: 16 May 2022

Atmospheric Measurement Techniques Discussions

Comparison of Two Photolytic Calibration Methods for Nitrous Acid

Andrew J. Lindsay and Ezra C. Wood

Department of Chemistry, Drexel University, Philadelphia, PA, USA

Correspondence to: Ezra C. Wood (ew456@drexel.edu)

Abstract. Nitrous acid (HONO) plays an important role in tropospheric oxidation chemistry as it is a precursor to the hydroxyl radical. Measurements of HONO have been historically difficult due to instrument interferences and difficulties in sampling and calibration. The traditional calibration method involves generation of HONO by reacting hydrogen chloride vapor with sodium nitrite followed by quantification by various methods (e.g., conversion of HONO to nitric oxide (NO) followed by chemiluminescence detection). Alternatively, HONO can be generated photolytically in the gas-phase by reacting NO with OH radicals generated by H_2O photolysis. In this work, we describe and compare two photolytic HONO calibration methods that were used to calibrate an iodide adduct chemical ionization mass spectrometer (CIMS). Both methods are based on the water vapor photolysis method commonly used for OH and HO_2 calibrations. The first method is an adaptation of the common chemical actinometry HOx calibration method, in which HONO is calculated based on quantified values for [O_3], [H_2O], [O_2], and the absorption cross sections for H_2O and O_2 at 184.9 nm. In the second, novel method the HONO concentration is simply determined based on the simultaneous measurements of NO_2 formed by the reaction of NO with HO_2 from the H_2O photolysis. This second, novel approach generally has an improved (lower) calibration uncertainty and is simpler to apply. Calibration uncertainties are typically 30 to 36% (2σ) for the actinometric method and as low as 9% (2σ) for the NO_2 proxy method, limited by the uncertainty of the NO_2 measurements.

1 Introduction

Nitrous acid (HONO) is a source of the most important atmospheric oxidant – the hydroxyl radical (OH) - and can therefore play an important role in tropospheric oxidation chemistry. The hydroxyl radical causes the removal of most trace gases from the atmosphere while initiating the formation of secondary pollutants such as ozone (O_3) and secondary organic aerosol (SOA). Photolysis of HONO yields OH and nitric oxide (NO):

$$HONO + h\nu \rightarrow OH + NO \quad (\lambda < 400\ nm) \qquad (R1)$$

This reaction is the primary sink of HONO during the daytime leading to a typical chemical lifetime at mid-day of between 10-20 minutes at mid-latitudes. Sources of HONO include homogeneous formation (R2), direct emissions from combustion (vehicles, biomass burning, etc.) and soils, and numerous heterogenous processes including heterogeneous reaction of NO_2 with moist terrestrial surfaces, photolysis of particulate nitrate (Ye et al., 2016;Ye et al., 2017), and photolysis of nitric acid (Ye et al., 2016).

$$OH + NO + M \rightarrow HONO + M \qquad (R2)$$

The relative importance of these sources varies with environment (Jiang et al., 2022).

HONO photolysis has been reported as a major source of HOx (HOx = OH + HO_2) throughout the day in a variety of environments, including urban and highly polluted areas (Whalley et al., 2018;Slater et al., 2020;Ren et al., 2013;Lu et al., 2019)

https://doi.org/10.5194/amt-2022-157
Preprint. Discussion started: 16 May 2022


Atmospheric Measurement Techniques Discussions

as well as more pristine environments (Villena et al., 2011;Jiang et al., 2020;Bloss et al., 2007). Vertical distributions of HONO, however, indicate that its significance as a HOx precursor may be limited to near ground level (Li et al., 2014;Young et al., 2012;Villena et al., 2011;Wong et al., 2012;Tuite et al., 2021;Jaeglé et al., 2018).

HONO is notoriously difficult to measure. It can be formed via heterogeneous chemistry within sampling lines or an instrument's inlet. The resulting interferences may pose additional challenges in applying an instrument's zero or in calibration processes that alter the interfering species. Some intercomparison studies have shown substantial differences between HONO measurement techniques. For a Beijing, China based study, a comparison of several HONO measurements showed an overall mixed agreement with major differences observed for a few techniques (Crilley et al., 2019). Measurements in Houston, Texas showed several instruments to mostly agree in capturing variations in HONO, though there were differences in the magnitude of presented [HONO] values (Pinto et al., 2014). Bourgeois et al. (in review, 2022) recently reported an 80% difference between HONO measurements made by cavity-enhanced spectroscopy and iodide-adduct chemical ionization mass spectrometry (CIMS). Closer agreement for two instrument HONO comparisons has been reported by Stutz et al. (2010) (comparing differential optical absorption spectroscopy (DOAS) and mist-chamber ion chromatography (IC)), Cheng et al. (2013) (comparing Long-path absorption photometry (LOPAP) and stripping coil IC), and Dixneuf et al. (2022) (comparing LOPAP and cavity-enhanced absorption spectroscopy), though many of these studies report considerable deviations when HONO mixing ratios were less than ~100 pptv.

Calibrations for HONO are challenging as it is not commercially available and rather must be prepared in situ. Most commonly, HONO is prepared by reacting hydrogen chloride vapor with sodium nitrite (Febo et al., 1995):

$$HCl_{(g)} + NaNO_{2(s)} \rightarrow HONO_{(g)} + NaCl_{(s)} \quad \text{(R3)}$$

This method presents several challenges. A stable source of HCl is required, usually from a heated aqueous solution, a gas cylinder, or a permeation tube. Consistent mixing between the HCl and the $NaNO_2$ powder is required. This method typically produces high HONO concentrations (above 1 ppmv), requiring dilution, though the temporary unrealistic HONO concentrations can lead to significant HONO loss by its self-reaction and inaccurate HONO quantification. The generated HONO can be quantified by various methods including conversion to NO followed by chemiluminescence detection (Lee et al., 2012;Lao et al., 2020;Villena and Kleffmann, 2022), thermal conversion to NO_2 followed by NO_2 quantification (Gingerysty and Osthoff, 2020), and conversion to aqueous nitrite followed by derivatization and detection by UV-vis (Peng et al., 2020).

More recently, photolytic HONO sources have been utilized. Humidified air is exposed to ultraviolet (UV) light to photolyze H_2O to produce an equal mixture of OH and HO_2, which in the presence of excess NO then converts to HONO. This HONO output is tunable by altering humidity, UV flux, or UV exposure time. The HONO formed has been quantified by inferring the UV flux by measuring the O_3 produced from O_2 photolysis (Dyson et al., 2021;Bottorff et al., 2021) and by thermal dissociation of the HONO followed by measurement of the NO_2 produced (Veres et al., 2015). These methods have an uncertainty of 30 to 36% (2σ), similar to the uncertainty for HOx calibrations based on water vapor photolysis (Dusanter et al., 2008). In this manuscript, we present an alternative photolytic HONO calibration that we refer to as the "NO_2 proxy" method. This method requires a direct NO_2 measurement that is used as a 'proxy' to quantify HONO concentrations. We compare this new proxy calibration to the more standard photolytic calibration method as performed by Bottorff et al. (2021) and Dyson et al. (2021). This method has a lower uncertainty (typically ~10%, 2σ) and unlike the actinometric method does not require characterization of the mercury lamp emission spectrum.

2 Methods

https://doi.org/10.5194/amt-2022-157
Preprint. Discussion started: 16 May 2022

Atmospheric Measurement Techniques Discussions

2.1 Instrumentation

A Cavity Attenuated Phase Shift (CAPS) spectrometer was used to detect NO_2 (Kebabian et al., 2008). The CAPS also indirectly measured O_3 as it was converted to NO_2 by reaction with excess NO. The CAPS instrument was calibrated using a 2B Technologies Model 306 O_3 Calibration Source, which agreed to within 2.5% with a Thermo Environmental Instruments 49C O_3 Calibrator. We assign an uncertainty of 3% (2σ) to the NO_2 measurements. Temperature and relative humidity (RH) measurements were made using two Vaisala HMP60 probes.

A High-Resolution Chemical Ionization Time of Flight Mass Spectrometer (HR-ToF-CIMS, Tofwerks/Aerodyne Research, Inc.) was used to detect HONO (Bertram et al., 2011;Lee et al., 2014). HONO and concomitant gases are ionized within a laboratory-built ion-molecule reactor (IMR) using reagent iodide (I^-) ions. The IMR is internally coated with PTFE and sampled the calibration gas at a flow rate of 2.10 SLPM through a stainless-steel critical orifice (nominal diameter of 0.48 mm). Iodide (I^-) reagent ions in N_2 were sampled at 2.20 SLPM through a similar critical orifice perpendicular to the main sample flow. The I^- was prepared by exposing dilute methyl iodide (CH_3I) from a permeation tube to a ^{210}Po radioactive source. Humidified N_2 was also added to the IMR perpendicular to the main sample flow at a flow rate of 0.365 SLPM. The pressure in the IMR was held at 80 mbar, controlled by adjusting a valve to the scroll pump (Agilent Technologies IDP-7).

Ions are separated by mass-to-charge ratio (m/z) at a mass resolving power of near 5000 m/Δm. We monitor the HONO iodide adduct $I(HONO)^-$ at 173.90575 m/z. The peak-fitting software (TofWare) accounts for the overlapping contribution from the ^{13}C formic acid $I(^{13}CH_2O_2)^-$ peak at 173.91342 m/z. We account for the humidity dependence of the instrumental response by determining the mole fraction of $H_2O_{(g)}$ (χ_{H2O}) in the IMR by measuring the RH and temperature of the IMR in the exhaust of the scroll pump.

2.2 Calibration Methods

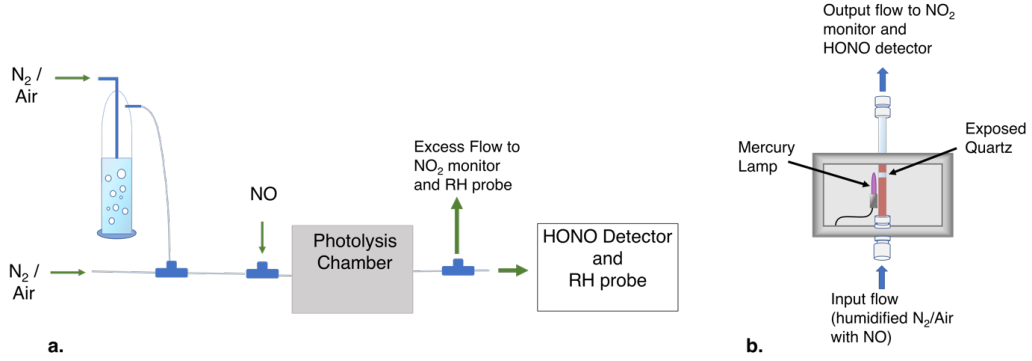

Figure 1: Schematic of the experimental setup (a.) and the photolysis chamber (b.). Not shown: small flow of air when using N_2 as the carrier gas (a.), and the purge flow of N_2 (b.).

We calibrate HONO using two variations of the water vapor HOx calibration method: one is a modification of the standard actinometric HOx photolytic calibration and the other we refer to as the "NO_2 proxy" calibration. These calibration methods mainly differ in how HONO is quantified. In both methods, HONO was produced nearly identically. Humidified air (for the actinometric method) or N_2 (for the NO_2 proxy calibration) is mixed with NO and then exposed to 184.9 nm ultraviolet radiation from a low-pressure mercury lamp (Jelight 78-2046-1). The resulting OH and HO_2 from water photolysis form HONO by reaction with excess NO (R4-6a and R2).

https://doi.org/10.5194/amt-2022-157
Preprint. Discussion started: 16 May 2022


Atmospheric Measurement Techniques Discussions

$H_2O + hv \rightarrow H + OH$ (R4)

$H + O_2 + M \rightarrow HO_2 + M$ (R5)

$HO_2 + NO \rightarrow OH + NO_2$ (R6a)

$OH + NO + M \rightarrow HONO + M$ (R2)

The HO_2 to HONO pathway is limited by the following reaction:

$HO_2 + NO + M \rightarrow HNO_3 + M$ (R6b)

A schematic of the setup used for both calibrations is shown in Figure 1. The mercury lamp is housed within a 10.8 cm × 26.7 cm × 10.2 cm photolysis chamber (Fig. 1b), and the volume surrounding the lamp is purged with dry N_2 (purge not shown). The humidified air-NO mixture is transported past the mercury lamp within a partially exposed 26.7 cm quartz tube (I.D. = 1.04 cm). HONO sample concentrations are controlled by adjusting the lamp flux with a Variac Variable transformer, adjusting the relative flow rates of the dry and humidified ZA/N_2, or adjusting the absolute flow rates to alter the lamp exposure time. For our example calibrations discussed in this manuscript, we typically used a main N_2 or air flow rate of 5 SLPM with an addition of 200 sccm of 41.02 ppmv NO in N_2 (Airgas) for a total flow rate of 5.20 SLPM and a diluted NO mixing ratio of 1.58 ppmv. Pseudo-first order rate constants calculated using this [NO] for R6a and R2 (the reactions that form HONO) are 322 s^{-1} and 295 s^{-1}, respectively. Under these conditions, HOx is converted to HONO within 0.02 s inside the remaining 11.4 cm of the quartz tube. The [NO] chosen must be high enough to minimize OH and HO_2 wall losses. We have ensured that this NO mixing ratio is sufficient in separate experiments by confirming that no additional HONO signal results at increased [NO] values.

The resulting calibration gas was sampled by the CIMS (2.1 SLPM) and the NO_2 monitor (1.1 SLPM). The excess flow was vented past an RH/T probe to determine the water mixing ratio in the photolysis cell. A second RH/T probe quantified the water mixing ratio in the CIMS IMR as previously mentioned in Sect. 2.1. Details of the two calibration methods are described in the following sections.

2.2.1 Actinometric Calibration

The water vapor photolysis calibration method has been used for several decades to calibrate OH and HO_2 measurements (Stevens et al., 1994;Lanzendorf et al., 1997;Dusanter et al., 2008). The concentration of HOx, and therefore HONO, is calculated from the time-integrated photolysis of water vapor:

$$[\mathrm{HONO}] \approx [\mathrm{HOx}] = (F \cdot t)[\mathrm{H_2O}]\sigma_{\mathrm{H_2O}}\phi_{\mathrm{HO_x}} \quad (1)$$

Where F is the photon flux at 184.9 nm, t is the UV irradiation time, σ_{H2O} is the absorption cross section of water at 184.9 nm, and Φ_{HOx} is the quantum yield of HOx from water photolysis and equal to 2. F can be quantified using direct actinometric measurements (e.g., using a calibrated phototube), and t can be quantified via characterization of the flow rates and photolysis cell geometry (Faloona et al., 2004). Alternatively, and more commonly among HOx measurement groups, the product $F{\cdot}t$ can be determined via "chemical actinometry" (Schultz et al., 1995). In the O_2-O_3 chemical actinometry method, the concentration of O_3 produced by photodissociation of O_2 at 184.9 is used to determine $F{\cdot}t$:

$O_2 + hv \rightarrow O + O$ (R7)

$O + O_2 + M \rightarrow O_3 + M$ (R8)

https://doi.org/10.5194/amt-2022-157
Preprint. Discussion started: 16 May 2022


Atmospheric Measurement Techniques Discussions

The product of the lamp flux and the exposure time, i.e., the ($F \cdot t$) term, is given by Eq. (2), in which σ_{O2} is the absorption cross section of O_2 at 184.9 nm and Φ_{O3} is quantum yield of O_3 from O_2 photolysis ($\Phi_{O2} = 2$):

$$(F \cdot t) = \frac{[O_3]}{[O_2]\sigma_{O_2}\phi_{O_3}} \quad (2)$$

Substituting this expression for $F \cdot t$ into Eq. (1) gives Eq. (3):

$$[HONO] \approx [HOx] = \frac{[O_3]}{[O_2]\sigma_{O_2}}[H_2O]\sigma_{H2O} \quad (3)$$

The effective value for σ_{O2} must be experimentally determined for the individual mercury lamp at the experimental O_2 optical depth to account for the non-ideal overlap between the lamp emission spectrum and the O_2 absorption spectrum (Lanzendorf et al., 1997). We use a value of 1.4 x 10^{-20} cm^2 $molec^{-1}$ for σ_{O2} for the mercury lamp used for these experiments. We use the JPL-recommended value of 7.1 x 10^{-20} cm^2 $molec^{-1}$ for σ_{H2O} (Burkholder et al., 2020).

We apply a small correction to the [HOx] calculated in Eq. (3) in order to obtain [HONO]. This correction accounts for the incomplete conversion of HO_2 to HONO due to R6b.

$$[HONO] = (0.5 + 0.5 \cdot (1 - \frac{\beta}{1+\beta})) \cdot [HOx] \quad (4)$$

Equation 4 includes the variable β, which is the relative rate or product ratio of R6b to R6a (i.e., $\beta = k_{R6b}/k_{R6a} = [HNO_3]/[NO_2]$) and depends on temperature, pressure, and humidity (Butkovskaya et al., 2007;Butkovskaya et al., 2009). The Eq. (4) fraction that includes β represents a traditional branching ratio (i.e., $k_{R6b}/(k_{R6a} + k_{R6b}) = [HNO_3]/([NO_2]+[HNO_3])$). Values of β are at most 0.04, leading to a 2% correction to equation 1. See Sect. S1 of the supplement for information regarding the formulation of Eq. (4) and the calculation of β.

The O_3 concentration within Eq. (3) is determined with the CAPS NO_2 monitor after its reaction with NO, forming NO_2. This is measured with dry air flowing in the photolysis chamber so that the NO_2 measured is solely from the reaction of NO with O_3 and not HO_2. $[H_2O]$ is determined using the measured RH, temperature, and pressure. The CIMS response to HONO is determined by acquiring a background by briefly toggling off the mercury lamp. This background CIMS signal is humidity dependent, so a background is taken at each humidity setting. The NO flow contributes to the CIMS background HONO signal but is constant over time.

2.2.2 Proxy Calibration

For the NO_2 proxy calibration method, we determine [HONO] from the measured value of $[NO_2]$ formed from R6a during HONO production. For each H_2O molecule photolyzed (R4), nearly one NO_2 and two HONO molecules are produced. Therefore, [HONO] is simply given by the measured $[NO_2]$ (Eq. (5)):

$$[HONO] = (2 + \beta) \cdot [NO_2] \quad (5)$$

Where β is added to account for the minor HNO_3 product of the HO_2 + NO reaction (R6b).

For the proxy calibration we use humidified N_2 rather than air and include a small addition of 10 sccm of zero air prior to lamp exposure (not shown in the schematic). The resulting low O_2 concentration is sufficient for the full conversion of H to HO_2 (R5) but results in a negligible amount of O_3 formed by O_2 photolysis (R7-R8), confirmed by toggling the UV source on and off with

https://doi.org/10.5194/amt-2022-157
Preprint. Discussion started: 16 May 2022


Atmospheric Measurement Techniques Discussions

dry N_2 flowing. HONO concentrations are quantified using background subtracted [NO_2] values in Eq. (5), which are typically acquired by toggling the mercury lamp off and on. The CIMS signal response is determined simultaneously.

3 Results and Discussion

Time series data for the proxy calibration method is shown in Fig. 2. The CAPS NO_2 measurement and the CIMS HONO signal normalized per one million counts of reagent ion per second ('ncps') are shown at a constant RH setting (40% within the H_2O photolysis cell). During the first 95 s, HONO is formed by H_2O photolysis via the mercury lamp 184.9 nm emission. This leads to the stable $I(HONO)^-$ signal in the CIMS along with enhanced [NO_2] produced by R6a and measured by the CAPS monitor. Background $I(HONO)^-$ and NO_2 signals are determined by toggling off the mercury lamp (shown at 96 s). The CIMS sensitivity (ncps ppt^{-1}) is equal to the quotient of the normalized background subtracted CIMS signal and the quantified [HONO] which is calculated by Eq. (5).

A multipoint NO_2 proxy calibration curve (Fig. 3) shows the linear CIMS signal response to [HONO]. This calibration was conducted at a constant relative humidity (28% within the photolysis cell and 18% within the CIMS IMR), and [HONO] was adjusted by altering the mercury lamp flux with a Variac variable transformer. The slope of this curve, 2.89 ± 0.34 ncps ppt^{-1} (2σ), is the CIMS sensitivity to HONO for this particular mole fraction of water within the CIMS IMR ($\chi_{H2O} = 3.88 \times 10^{-3}$). HONO mixing ratios ranged from approximately 400 pptv to 3500 pptv, thus demonstrating that a wide range in HONO concentrations can easily be prepared. The uncertainty for the quantified [HONO] from Eq. (5) (i.e., the x-error bars) is obtained by adding in quadrature three terms: 1.) the relative uncertainty of the NO_2 background subtraction (based on the 5 s average precision of 27 pptv), 2.) the NO_2 calibration uncertainty (3%, 2σ), and finally 3.) the relative error associated with the $(2+\beta)$ expression (typically 0.14%, 2σ). The uncertainty in the normalized CIMS signal is obtained by adding in quadrature the precision of the $I(HONO)^-$ signal with that of the reagent ion. The 2 σ error bars range from 5.6 to 34.8% for quantified [HONO] and 6.8 to 11.2% in the CIMS HONO signal. The Fig. 3 slope (i.e., the CIMS sensitivity to HONO) and its uncertainty was determined using the York bivariate linear regression method (York et al., 2004). The uncertainty calculations are discussed in greater detail in Sect. S2.1 of the supplement.

A comparison between the more standard O_3 actinometry based calibration and the new proxy calibration method is shown in Fig. 4. CIMS sensitivities as determined by single point calibrations are shown for a variety of χ_{H2O} values. The two calibration methods were conducted consecutively and agree within their provided 2σ errors. Sensitivities ranged from 1.5 to 5 ncps ppt^{-1} with the greatest values observed at low χ_{H2O} settings. The sensitivity determined by the Fig. 3 multipoint calibration (2.89 ± 0.34 ncps ppt^{-1} at $\chi_{H2O} = 3.88 \times 10^{-3}$) is consistent with those shown in Fig. 4 at similar χ_{H2O} values. These CIMS sensitivities are also in line with literature values (Peng et al., 2020;Bourgeois et al., in review, 2022). Unique to this figure is the use of the CIMS IMR χ_{H2O} to track humidity dependence rather than the partial pressure of H_2O (Lee et al., 2014) or the CIMS signal ratio of the iodide water adduct $I(H_2O)^-$ (m/z 145) to reagent ion I^- (m/z 127) (Lee et al., 2014;Peng et al., 2020;Veres et al., 2015;Veres et al., 2020). The use of χ_{H2O} allows for a more direct comparison to other CIMS users that may use different IMR pressures and quadrupole voltage settings that govern the $I(H_2O)^-$ to I^- ratio.

The uncertainty in CIMS sensitivity for the proxy method is determined by combining in quadrature the relative error of the background subtracted CIMS signal with that of the quantified [HONO] value. The calculation for quantified [HONO] uncertainty and CIMS uncertainty is previously mentioned in the text regarding Fig. 3, though the CIMS uncertainty here slightly differs due to the background subtraction (see Sect. S2.2 the supplement). As mentioned previously, the total uncertainty is dependent on the

https://doi.org/10.5194/amt-2022-157
Preprint. Discussion started: 16 May 2022

Atmospheric Measurement Techniques Discussions

quantified [HONO] value, which ranged from 630 (at the lowest χ_{H2O} value) to 7,800 pptv (at the greatest χ_{H2O} value) for the shown Fig. 4 proxy calibration results. The uncertainty at the lowest χ_{H2O} settings, which were also the lowest HONO concentrations, were dominated by [HONO] quantification stemming from the background subtraction of NO_2. Therefore, the uncertainty can be minimized by using higher HONO concentrations. The presented 2σ uncertainty in using the proxy method ranged from 8.7 to 38.8%. All presented proxy calibration uncertainties besides the two at lowest χ_{H2O} values (i.e., the smallest [HONO] values) fall well below the 30% 2σ uncertainty associated with the standard O_3 actinometry calibration. The proxy calibration is therefore a general improvement over the standard actinometry calibration, especially at high [HONO] values.

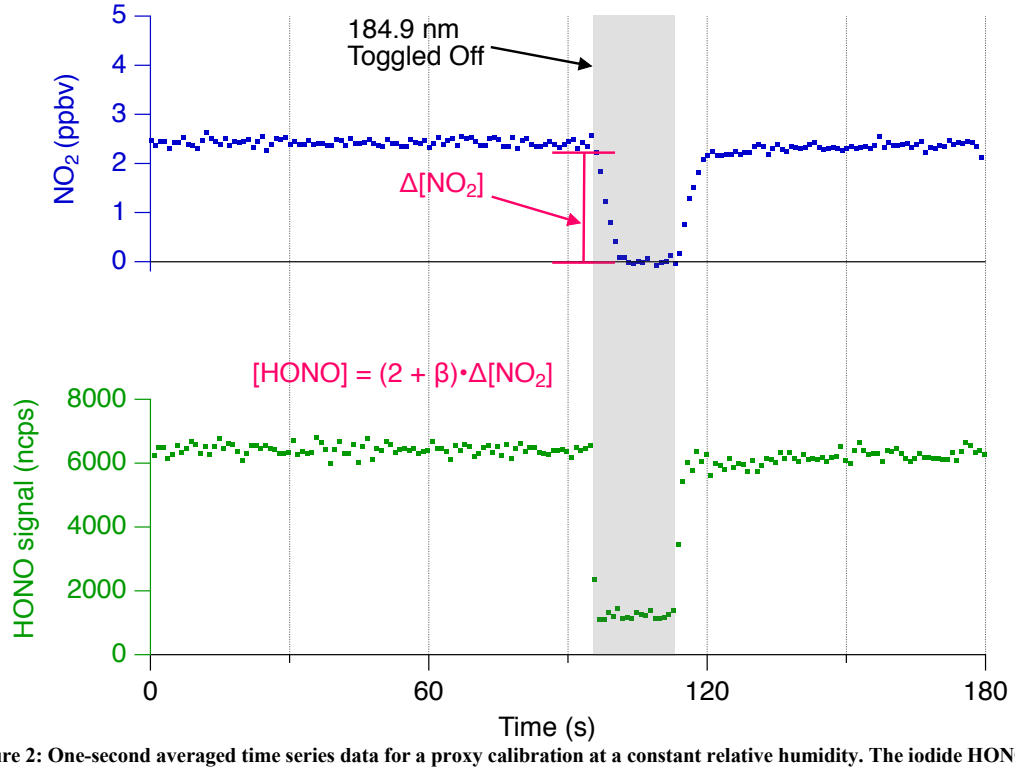

Figure 2: One-second averaged time series data for a proxy calibration at a constant relative humidity. The iodide HONO adduct signal (cps) is shown normalized per one million reagent ions (ncps). The highlighted section represents the period in which the 184.9 nm mercury lamp is toggled off to obtain background [NO_2] and HONO signal.

https://doi.org/10.5194/amt-2022-157
Preprint. Discussion started: 16 May 2022

Atmospheric Measurement Techniques Discussions

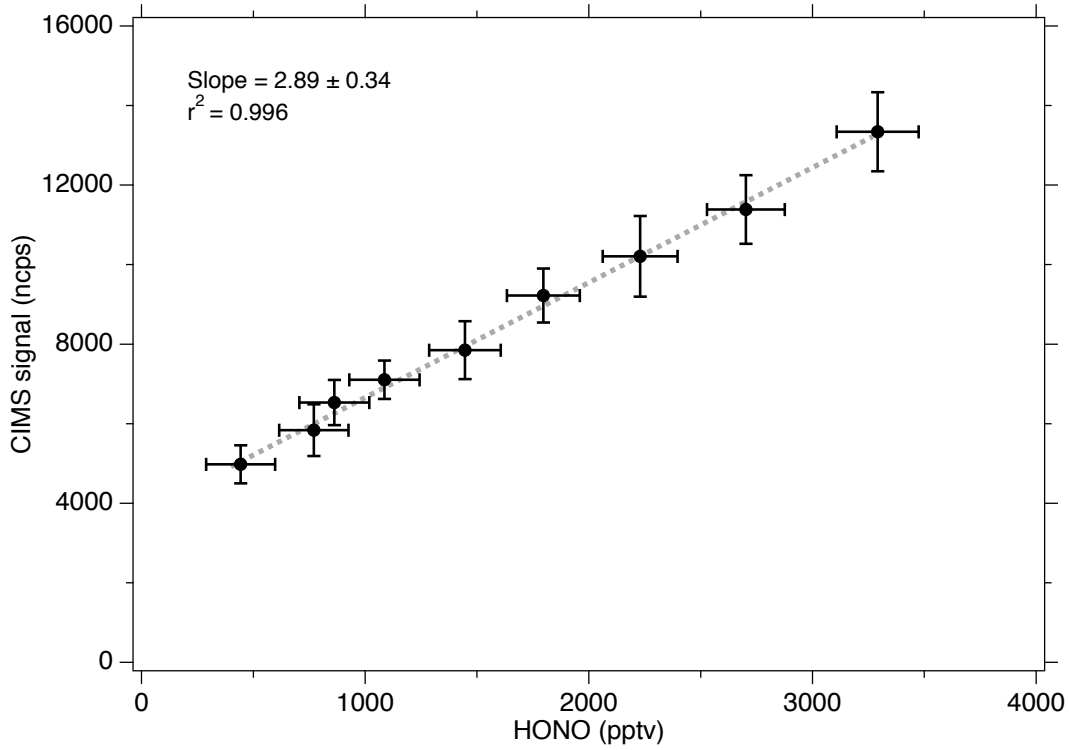

220 **Figure 3: Calibration curve obtained using the NO_2 proxy calibration method at a constant humidity (RH = 17.7%, [H_2O] = 0.388% as measured in the CIMS scroll pump exhaust). Error bars represent ± 2 σ.**

https://doi.org/10.5194/amt-2022-157
Preprint. Discussion started: 16 May 2022

Atmospheric Measurement Techniques Discussions

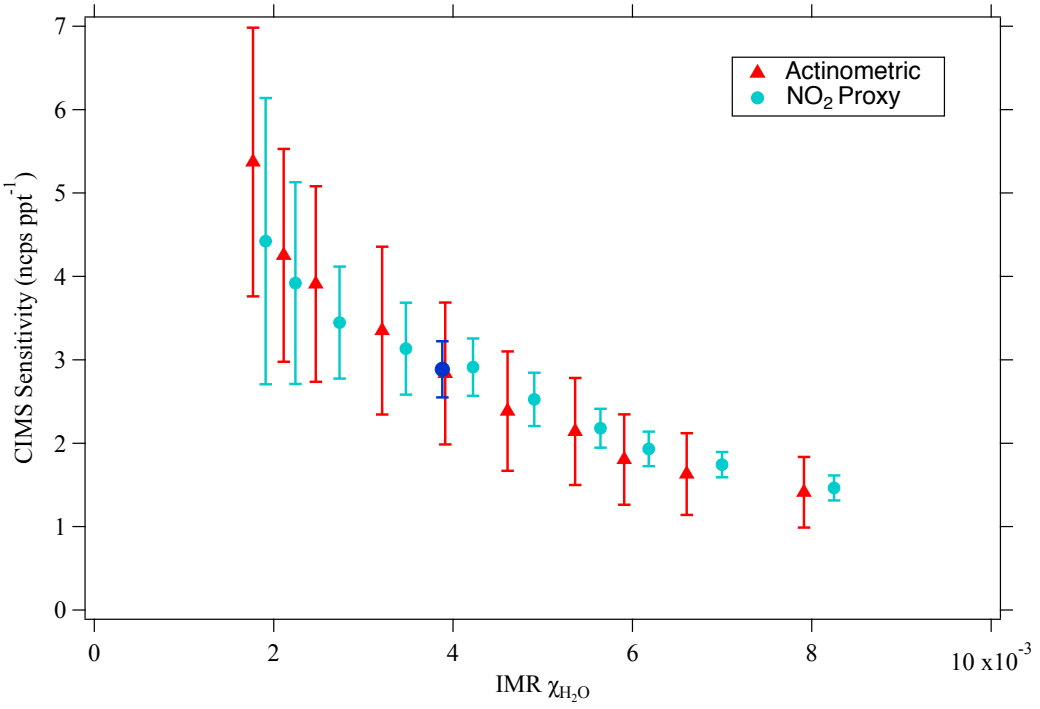

Figure 4: Comparison of the two HONO calibration methods for a range of χ_{H2O} within the CIMS IMR. The sensitivity determined by multipoint calibration (i.e., the Fig. 3 slope) is plotted as the dark blue circle. Error bars represent ± 2 σ.

4 Conclusions

Two photolytic HONO calibration methods based on reacting NO with the HOx generated by H_2O photolysis at 184.9 nm were presented. This includes a novel approach in which HONO is quantified using the NO_2 formed by the HO_2 + NO reaction as a proxy. The proxy method compares well with the O_3 actinometry based calibration while also having the benefit of a simpler calculation that avoids the need to characterize the emission spectrum of the mercury lamp used. In addition, this proxy method generally has improved uncertainties, typically between 8 and 20% (2σ) – lower than the 30 to 36% 2σ uncertainty associated with the actinometric calibration method. These photolytic calibrations require a direct NO_2 measurement (e.g., CAPS or CRDS), a 184.9 nm light source, and a simple quartz tube photolysis chamber. While the proxy calibration method was conducted in N_2 for this manuscript, it is possible to instead perform this method using air in the case that N_2 is incompatible with an instrument (unlike our CIMS). In an air-based proxy calibration, the [O_3] produced by O_2 photolysis would need to be quantified (during dry conditions) and then subtracted from subsequent background subtracted NO_2 signals. In conclusion, these photolytic calibration techniques offer a valuable alternative to the more conventional HONO calibration that is based on reacting hydrogen chloride vapor with sodium nitrite.

Data availability. The data used in this manuscript is available upon request.

https://doi.org/10.5194/amt-2022-157
Preprint. Discussion started: 16 May 2022

Atmospheric Measurement Techniques Discussions

Author contributions. AJL and ECW designed the experiments. AJL carried them out and performed the data analysis. AJL prepared the manuscript with contributions from ECW.

Competing Interests. The authors declare that they have no conflict of interest.

Acknowledgements. We acknowledge financial support from Directorate for Geosciences of the National Science Foundation. This work was supported by NSF grant AGS-2002928. We are grateful to Phil Stevens (Indiana University) for characterizing the mercury lamp used for these calibrations.

References

Bertram, T., Kimmel, J., Crisp, T., Ryder, O., Yatavelli, R., Thornton, J., Cubison, M., Gonin, M., and Worsnop, D.: A field-deployable, chemical ionization time-of-flight mass spectrometer, Atmospheric Measurement Techniques, 4, 1471-1479, https://doi.org/10.5194/amt-4-1471-2011, 2011.

Bloss, W., Lee, J., Heard, D., Salmon, R. A., Bauguitte, S.-B., Roscoe, H., and Jones, A.: Observations of OH and HO 2 radicals in coastal Antarctica, Atmospheric Chemistry and Physics, 7, 4171-4185, https://doi.org/10.5194/acp-7-4171-2007, 2007.

Bottorff, B., Reidy, E., Mielke, L., Dusanter, S., and Stevens, P. S.: Development of a laser-photofragmentation laser-induced fluorescence instrument for the detection of nitrous acid and hydroxyl radicals in the atmosphere, Atmospheric Measurement Techniques, 14, 6039-6056, https://doi.org/10.5194/amt-14-6039-2021, 2021.

Bourgeois, I., Peischl, J., Neuman, J. A., Brown, S. S., Allen, H. M., Campuzano-Jost, P., Coggon, M. M., DiGangi, J. P., Diskin, G. S., Gilman, J. B., Gkatzelis, G. I., Guo, H., Halliday, H., Hanisco, T. F., Holmes, C. D., Huey, L. G., Jimenez, J. L., Lamplugh, A. D., Lee, Y. R., Lindaas, J., Moore, R. H., Nowak, J. B., Pagonis, D., Rickly, P. S., Robinson, M. A., Rollins, A. W., Selimovic, V., St. Clair, J. M., Tanner, D., Vasquez, K. T., Veres, P. R., Warneke, C., Wennberg, P. O., Washenfelder, R. A., Wiggins, E. B., Womack, C. C., Xu, L., Zarzana, K. J., and Ryerson, T. B.: Comparison of airborne measurements of NO, NO2, HONO, NOy and CO during FIREX-AQ, https://doi.org/10.5194/amt-2021-432, in review, 2022.

Burkholder, J., Sander, S., Abbatt, J., Barker, J., Cappa, C., Crounse, J., Dibble, T., Huie, R., Kolb, C., and Kurylo, M.: Chemical kinetics and photochemical data for use in atmospheric studies, Evaluation No. 19, JPL Publication 19-10, Jet Propulsion Laboratory, Pasadena, 583-586, 2020.

Butkovskaya, N., Kukui, A., and Le Bras, G.: HNO3 Forming Channel of the HO2+ NO Reaction as a Function of Pressure and Temperature in the Ranges of 72− 600 Torr and 223− 323 K, The Journal of Physical Chemistry A, 111, 9047-9053, https://doi.org/10.1021/jp074117m, 2007.

Butkovskaya, N., Rayez, M.-T., Rayez, J.-C., Kukui, A., and Le Bras, G.: Water vapor effect on the HNO3 yield in the HO2+ NO reaction: experimental and theoretical evidence, The Journal of Physical Chemistry A, 113, 11327-11342, https://doi.org/10.1021/jp811428p, 2009.

Cheng, P., Cheng, Y., Lu, K., Su, H., Yang, Q., Zou, Y., Zhao, Y., Dong, H., Zeng, L., and Zhang, Y.: An online monitoring system for atmospheric nitrous acid (HONO) based on stripping coil and ion chromatography, Journal of Environmental Sciences, 25, 895-907, https://doi.org/10.1016/s1001-0742(12)60251-4, 2013.

Crilley, L. R., Kramer, L. J., Ouyang, B., Duan, J., Zhang, W., Tong, S., Ge, M., Tang, K., Qin, M., Xie, P., Shaw, M. D., Lewis, A. C., Mehra, A., Bannan, T. J., Worrall, S. D., Priestley, M., Bacak, A., Coe, H., Allan, J., Percival, C. J., Popoola, O. A. M.,

Jones, R. L., and Bloss, W. J.: Intercomparison of nitrous acid (HONO) measurement techniques in a megacity (Beijing), Atmospheric Measurement Techniques, 12, 6449-6463, https://doi.org/10.5194/amt-12-6449-2019, 2019.

Dixneuf, S., Ruth, A. A., Häseler, R., Brauers, T., Rohrer, F., and Dorn, H.-P.: Detection of nitrous acid in the atmospheric simulation chamber SAPHIR using open-path incoherent broadband cavity-enhanced absorption spectroscopy and extractive long-path absorption photometry, Atmospheric Measurement Techniques, 15, 945-964, https://doi.org/10.5194/amt-15-945-2022, 2022.

Dusanter, S., Vimal, D., and Stevens, P.: Measuring tropospheric OH and HO 2 by laser-induced fluorescence at low pressure. A comparison of calibration techniques, Atmospheric Chemistry and Physics, 8, 321-340, https://doi.org/10.5194/acp-8-321-2008, 2008.

Dyson, J. E., Boustead, G. A., Fleming, L. T., Blitz, M., Stone, D., Arnold, S. R., Whalley, L. K., and Heard, D. E.: Production of HONO from NO 2 uptake on illuminated TiO 2 aerosol particles and following the illumination of mixed TiO 2⁄ammonium nitrate particles, Atmospheric Chemistry and Physics, 21, 5755-5775, https://doi.org/10.5194/acp-21-5755-2021, 2021.

Faloona, I. C., Tan, D., Lesher, R. L., Hazen, N. L., Frame, C. L., Simpas, J. B., Harder, H., Martinez, M., Di Carlo, P., and Ren, X.: A laser-induced fluorescence instrument for detecting tropospheric OH and HO2: Characteristics and calibration, Journal of Atmospheric Chemistry, 47, 139-167, https://doi.org/10.1023/B:JOCH.0000021036.53185.0e, 2004.

Febo, A., Perrino, C., Gherardi, M., and Sparapani, R.: Evaluation of a high-purity and high-stability continuous generation system for nitrous acid, Environmental science & technology, 29, 2390-2395, https://doi.org/10.1021/es00009a035, 1995.

Gingerysty, N. J., and Osthoff, H. D.: A compact, high-purity source of HONO validated by Fourier transform infrared and thermal-dissociation cavity ring-down spectroscopy, Atmospheric Measurement Techniques, 13, 4159-4167, https://doi.org/10.5194/amt-13-4159-2020, 2020.

Jaeglé, L., Shah, V., Thornton, J., Lopez-Hilfiker, F., Lee, B., McDuffie, E., Fibiger, D., Brown, S., Veres, P., and Sparks, T.: Nitrogen oxides emissions, chemistry, deposition, and export over the Northeast United States during the WINTER aircraft campaign, Journal of Geophysical Research: Atmospheres, 123, 12,368-312,393, https://doi.org/10.1029/2018JD029133, 2018.

Jiang, Y., Xue, L., Gu, R., Jia, M., Zhang, Y., Wen, L., Zheng, P., Chen, T., Li, H., and Shan, Y.: Sources of nitrous acid (HONO) in the upper boundary layer and lower free troposphere of the North China Plain: insights from the Mount Tai Observatory, Atmospheric Chemistry and Physics, 20, 12115-12131, https://doi.org/10.5194/acp-20-12115-2020, 2020.

Kebabian, P. L., Wood, E. C., Herndon, S. C., and Freedman, A.: A practical alternative to chemiluminescence-based detection of nitrogen dioxide: Cavity attenuated phase shift spectroscopy, Environmental science & technology, 42, 6040-6045, https://doi.org/10.1021/es703204j, 2008.

Lanzendorf, E., Hanisco, T., Donahue, N., and Wennberg, P.: Comment on:"The measurement of tropospheric OH radicals by laser-induced fluorescence spectroscopy during the POPCORN Field Campaign" by Hofzumahaus et al. and "Intercomparison of tropospheric OH radical measurements by multiple folded long-path laser absorption and laser induced fluorescence" by Brauers et al, Geophysical research letters, 24, 3037-3038, https://doi.org/10.1029/97GL02899, 1997.

Lao, M., Crilley, L. R., Salehpoor, L., Furlani, T. C., Bourgeois, I., Neuman, J. A., Rollins, A. W., Veres, P. R., Washenfelder, R. A., Womack, C. C., Young, C. J., and VandenBoer, T. C.: A portable, robust, stable, and tunable calibration source for gas-phase nitrous acid (HONO), Atmospheric Measurement Techniques, 13, 5873-5890, https://doi.org/10.5194/amt-13-5873-2020, 2020.

Lee, B., Wood, E., Wormhoudt, J., Shorter, J., Herndon, S., Zahniser, M., and Munger, J.: Effective line strengths of trans-nitrous acid near 1275 cm− 1 and cis-nitrous acid at 1660 cm− 1, Journal of Quantitative Spectroscopy and Radiative Transfer, 113, 1905-1912, https://doi.org/10.1016/j.jqsrt.2012.06.004, 2012.

Lee, B. H., Lopez-Hilfiker, F. D., Mohr, C., Kurtén, T., Worsnop, D. R., and Thornton, J. A.: An iodide-adduct high-resolution time-of-flight chemical-ionization mass spectrometer: Application to atmospheric inorganic and organic compounds, Environmental science & technology, 48, 6309-6317, https://doi.org/10.1021/es500362a, 2014.

Li, X., Rohrer, F., Hofzumahaus, A., Brauers, T., Häseler, R., Bohn, B., Broch, S., Fuchs, H., Gomm, S., and Holland, F.: Missing gas-phase source of HONO inferred from Zeppelin measurements in the troposphere, Science, 344, 292-296, https://doi.org/10.1126/science.1248999, 2014.

Lu, K., Fuchs, H., Hofzumahaus, A., Tan, Z., Wang, H., Zhang, L., Schmitt, S. H., Rohrer, F., Bohn, B., and Broch, S.: Fast photochemistry in wintertime haze: consequences for pollution mitigation strategies, Environmental science & technology, 53, 10676-10684, https://doi.org/10.1021/acs.est.9b02422, 2019.

Peng, Q., Palm, B. B., Melander, K. E., Lee, B. H., Hall, S. R., Ullmann, K., Campos, T., Weinheimer, A. J., Apel, E. C., and Hornbrook, R. S.: HONO emissions from western US wildfires provide dominant radical source in fresh wildfire smoke, Environmental science & technology, 54, 5954-5963, https://doi.org/10.1021/acs.est.0c00126, 2020.

Pinto, J. P., Dibb, J., Lee, B. H., Rappenglück, B., Wood, E. C., Levy, M., Zhang, R. Y., Lefer, B., Ren, X. R., Stutz, J., Tsai, C., Ackermann, L., Golovko, J., Herndon, S. C., Oakes, M., Meng, Q. Y., Munger, J. W., Zahniser, M., and Zheng, J.: Intercomparison of field measurements of nitrous acid (HONO) during the SHARP campaign, Journal of Geophysical Research: Atmospheres, 119, 5583-5601, https://doi.org/10.1002/2013jd020287, 2014.

Ren, X., Van Duin, D., Cazorla, M., Chen, S., Mao, J., Zhang, L., Brune, W. H., Flynn, J. H., Grossberg, N., and Lefer, B. L.: Atmospheric oxidation chemistry and ozone production: Results from SHARP 2009 in Houston, Texas, Journal of Geophysical Research: Atmospheres, 118, 5770-5780, https://doi.org/10.1002/jgrd.50342, 2013.

Schultz, M., Heitlinger, M., Mihelcic, D., and Volz-Thomas, A.: Calibration source for peroxy radicals with built-in actinometry using H2O and O2 photolysis at 185 nm, Journal of Geophysical Research: Atmospheres, 100, 18811-18816, https://doi.org/10.1029/95JD01642, 1995.

Slater, E. J., Whalley, L. K., Woodward-Massey, R., Ye, C., Lee, J. D., Squires, F., Hopkins, J. R., Dunmore, R. E., Shaw, M., and Hamilton, J. F.: Elevated levels of OH observed in haze events during wintertime in central Beijing, Atmospheric Chemistry and Physics, 20, 14847-14871, https://doi.org/10.5194/acp-20-14847-2020, 2020.

Stevens, P., Mather, J., and Brune, W.: Measurement of tropospheric OH and HO2 by laser-induced fluorescence at low pressure, Journal of Geophysical Research: Atmospheres, 99, 3543-3557, https://doi.org/10.1029/93JD03342, 1994.

Stutz, J., Oh, H.-J., Whitlow, S. I., Anderson, C., Dibb, J. E., Flynn, J. H., Rappenglück, B., and Lefer, B.: Simultaneous DOAS and mist-chamber IC measurements of HONO in Houston, TX, Atmospheric Environment, 44, 4090-4098, https://doi.org/10.1016/j.atmosenv.2009.02.003, 2010.

Tuite, K., Thomas, J. L., Veres, P. R., Roberts, J. M., Stevens, P. S., Griffith, S. M., Dusanter, S., Flynn, J. H., Ahmed, S., and Emmons, L.: Quantifying nitrous acid formation mechanisms using measured vertical profiles during the CalNex 2010 campaign and 1D column modeling, Journal of Geophysical Research: Atmospheres, 126, e2021JD034689, https://doi.org/10.1029/2021JD034689, 2021.

Veres, P. R., Roberts, J. M., Wild, R. J., Edwards, P. M., Brown, S. S., Bates, T. S., Quinn, P. K., Johnson, J. E., Zamora, R. J., and de Gouw, J.: Peroxynitric acid (HO2NO2) measurements during the UBWOS 2013 and 2014 studies using iodide ion

chemical ionization mass spectrometry, Atmospheric Chemistry and Physics, 15, 8101-8114, https://doi.org/10.5194/acp-15-8101-2015, 2015.

Veres, P. R., Neuman, J. A., Bertram, T. H., Assaf, E., Wolfe, G. M., Williamson, C. J., Weinzierl, B., Tilmes, S., Thompson, C. R., and Thames, A. B.: Global airborne sampling reveals a previously unobserved dimethyl sulfide oxidation mechanism in the marine atmosphere, Proceedings of the National Academy of Sciences, 117, 4505-4510, https://doi.org/10.1073/pnas.1919344117, 2020.

Villena, G., Kleffmann, J., Kurtenbach, R., Wiesen, P., Lissi, E., Rubio, M. A., Croxatto, G., and Rappenglück, B.: Vertical gradients of HONO, NOx and O3 in Santiago de Chile, Atmospheric Environment, 45, 3867-3873, https://doi.org/10.1016/j.atmosenv.2011.01.073, 2011.

Villena, G., and Kleffmann, J.: A source for the continuous generation of pure and quantifiable HONO mixtures, Atmospheric Measurement Techniques, 15, 627-637, https://doi.org/10.5194/amt-15-627-2022, 2022.

Whalley, L. K., Stone, D., Dunmore, R., Hamilton, J., Hopkins, J. R., Lee, J. D., Lewis, A. C., Williams, P., Kleffmann, J., and Laufs, S.: Understanding in situ ozone production in the summertime through radical observations and modelling studies during the Clean air for London project (ClearfLo), Atmospheric Chemistry and Physics, 18, 2547-2571, https://doi.org/10.5194/acp-18-2547-2018, 2018.

Wong, K., Tsai, C., Lefer, B., Haman, C., Grossberg, N., Brune, W., Ren, X., Luke, W., and Stutz, J.: Daytime HONO vertical gradients during SHARP 2009 in Houston, TX, Atmospheric Chemistry and Physics, 12, 635-652, https://doi.org/10.5194/acp-12-635-2012, 2012.

Ye, C., Gao, H., Zhang, N., and Zhou, X.: Photolysis of Nitric Acid and Nitrate on Natural and Artificial Surfaces, Environ Sci Technol, 50, 3530-3536, https://doi.org/10.1021/acs.est.5b05032, 2016.

Ye, C., Zhang, N., Gao, H., and Zhou, X.: Photolysis of Particulate Nitrate as a Source of HONO and NOx, Environ Sci Technol, 51, 6849-6856, https://doi.org/10.1021/acs.est.7b00387, 2017.

York, D., Evensen, N. M., Martınez, M. L., and De Basabe Delgado, J.: Unified equations for the slope, intercept, and standard errors of the best straight line, American Journal of Physics, 72, 367-375, https://doi.org/10.1119/1.1632486, 2004.

Young, C. J., Washenfelder, R. A., Roberts, J. M., Mielke, L. H., Osthoff, H. D., Tsai, C., Pikelnaya, O., Stutz, J., Veres, P. R., Cochran, A. K., VandenBoer, T. C., Flynn, J., Grossberg, N., Haman, C. L., Lefer, B., Stark, H., Graus, M., de Gouw, J., Gilman, J. B., Kuster, W. C., and Brown, S. S.: Vertically resolved measurements of nighttime radical reservoirs in Los Angeles and their contribution to the urban radical budget, Environ Sci Technol, 46, 10965-10973, https://doi.org/10.1021/es302206a, 2012.